Title

Exploring the molecular basis for substrate specificity in homologous macrolide biosynthetic cytochromes P450

Journal

Journal of Biological Chemistry, 294(44)

ISSN

0021-9258

Authors

DeMars, Matthew D
Samora, Nathan L
Yang, Song
et al.

Publication Date

2019-11-01

DOI

10.1074/jbc.ra119.010352

Exploring the molecular basis for substrate specificity in homologous macrolide biosynthetic cytochromes P450

Received for publication, July 24, 2019, and in revised form, August 30, 2019 Published, Papers in Press, September 5, 2019, DOI 10.1074/jbc.RA119.010352

Matthew D. DeMars II[‡1], Nathan L. Samora[§], Song Yang[¶], Marc Garcia-Borràs[¶], Jacob N. Sanders[¶], K. N. Houk[¶], Larissa M. Podust[§], and David H. Sherman[‡‖**‡‡2]

*From the [‡]Life Sciences Institute and Departments of [‖]Medicinal Chemistry, **Chemistry, and [‡‡]Microbiology and Immunology, University of Michigan, Ann Arbor, Michigan 48109, [§]Skaggs School of Pharmacy and Pharmaceutical Sciences, University of California, San Diego, California 92093, and [¶]Department of Chemistry and Biochemistry, University of California, Los Angeles, California 90095*

Edited by John M. Denu

Cytochromes P450 (P450s) are nature's catalysts of choice for performing demanding and physiologically vital oxidation reactions. Biochemical characterization of these enzymes over the past decades has provided detailed mechanistic insight and highlighted the diversity of substrates P450s accommodate and the spectrum of oxidative transformations they catalyze. Previously, we discovered that the bacterial P450 MycCI from the mycinamicin biosynthetic pathway in *Micromonospora griseorubida* possesses an unusually broad substrate scope, whereas the homologous P450 from tylosin-producing *Streptomyces fradiae* (TylHI) exhibits a high degree of specificity for its native substrate. Here, using biochemical, structural, and computational approaches, we aimed to understand the molecular basis for the disparate reactivity profiles of these two P450s. Turnover and equilibrium binding experiments with substrate analogs revealed that TylHI strictly prefers 16-membered ring macrolides bearing the deoxyamino sugar mycaminose. To help rationalize these results, we solved the X-ray crystal structure of TylHI in complex with its native substrate at 1.99-Å resolution and assayed several site-directed mutants. We also conducted molecular dynamics simulations of TylHI and MycCI and biochemically characterized a third P450 homolog from the chalcomycin biosynthetic pathway in *Streptomyces bikiniensis*. These studies provided a basis for constructing P450 chimeras to gain further insight into the features dictating the differences in reaction profile among these structurally and functionally related enzymes, ultimately unveiling the central roles of key loop regions in influencing substrate binding and turnover. Our work highlights the complex nature of P450/substrate interactions and raises interesting questions regarding the evolution of functional diversity among biosynthetic enzymes.

Since their discovery in the 1950s as components of mammalian liver microsomes (1–3), thousands of unique cytochrome P450 enzymes (P450s)[3] have been identified across all domains of life. P450s are heme-thiolate proteins, and every structurally characterized member of this superfamily adopts the same triangular prism-like fold (4, 5). Most P450s also share a common mechanism of dioxygen activation and typically act via a radical pathway to insert a single atom of oxygen into a C–H bond of a target substrate (6, 7). However, the nature of their catalytic cycle renders these enzymes capable of effecting a broad array of reactions, including epoxidation, heteroatom oxidation, dealkylation, oxidative aryl/phenolic coupling, and C–C bond formation/cleavage among many others (8–11). From a functional perspective, P450s play critical roles in cellular metabolism, ranging from xenobiotic metabolism in humans to secondary metabolite biosynthesis in plants, fungi, and bacteria.

The abundance of genes that encode P450s in microorganisms underscores the importance of this class of enzymes in catalyzing key biochemical steps in primary and secondary metabolic pathways (4). *Streptomyces* species are particularly rich sources of natural products possessing a range of biological activities (*e.g.* antibacterial, antifungal, antitumor, and immunosuppressive). P450s have been identified to play key roles in the biosynthesis of many of these compounds, often contribut-

This work was supported by the National Science Foundation under Center for Chemical Innovation Center for Selective C–H Functionalization Grant CHE-1700982, National Institutes of Health Grant R35-GM118101, and the Hans W. Vahlteich Professorship (to D. H. S.). The authors declare that they have no conflicts of interest with the contents of this article. The content is solely the responsibility of the authors and does not necessarily represent the official views of the National Institutes of Health.

This article contains Scheme S1, Tables S1-S6, Figs. S1-S9, supporting materials and methods, supplemental results, and NMR and HRMS data for newly reported compounds.

The atomic coordinates and structure factors (code 6B11) have been deposited in the Protein Data Bank (http://wwpdb.org/).

[1] Supported by the University of Michigan Cellular Biotechnology Training Program (National Institutes of Health Grant T32-GM008353) and a University of Michigan Rackham Predoctoral Fellowship. Present address: Dept. of Natural Product Biosynthesis, Max Planck Institute for Chemical Ecology, D-07745 Jena, Germany.

[2] To whom correspondence should be addressed: Life Sciences Institute, University of Michigan, Ann Arbor, MI 48109. Tel.: 734-615-9907; E-mail: davidhs@umich.edu.

[3] The abbreviations used are: P450, cytochrome P450; TylHI, 23-deoxy-5-*O*-mycaminosyl-tylonolide C23 hydroxylase from *S. fradiae*; MycCI, mycinamicin VIII C21 hydroxylase from *M. griseorubida*; ChmHI, 5-*O*-chalcosyl-chalconolide C20 hydroxylase from *S. bikiniensis*; TylHII, TylHI-associated ferredoxin; MycCII, MycCI-associated ferredoxin; ChmHII, ChmHI-associated ferredoxin; MBP-FdR, maltose-binding protein–tagged spinach ferredoxin reductase; RhFRED, reductase domain of $P450_{RhF}$ from *Rhodococcus* sp. NCIMB 9784; MD, molecular dynamics; SRS, substrate recognition site; PDB, Protein Data Bank; MT, 5-*O*-mycaminosyl-tylactone; 23-DMTL, 23-deoxy-5-*O*-mycaminosyl-tylonolide; MTL, 5-*O*-mycaminosyl-tylonolide; DT, 5-*O*-desosaminyl-tylactone; 23-DDTL, 23-deoxy-5-*O*-desosaminyl-tylonolide; 20-OH-MT, 20-hydroxy-5-*O*-mycaminosyl-tylactone; 20-OH-DT, 20-hydroxy-5-*O*-desosaminyl-tylactone; M-VIII, mycinamicin VIII; PML-IV, protomycinolide IV; Tyl, tylosin; Myc, mycinamicin; Chm, chalcomycin.

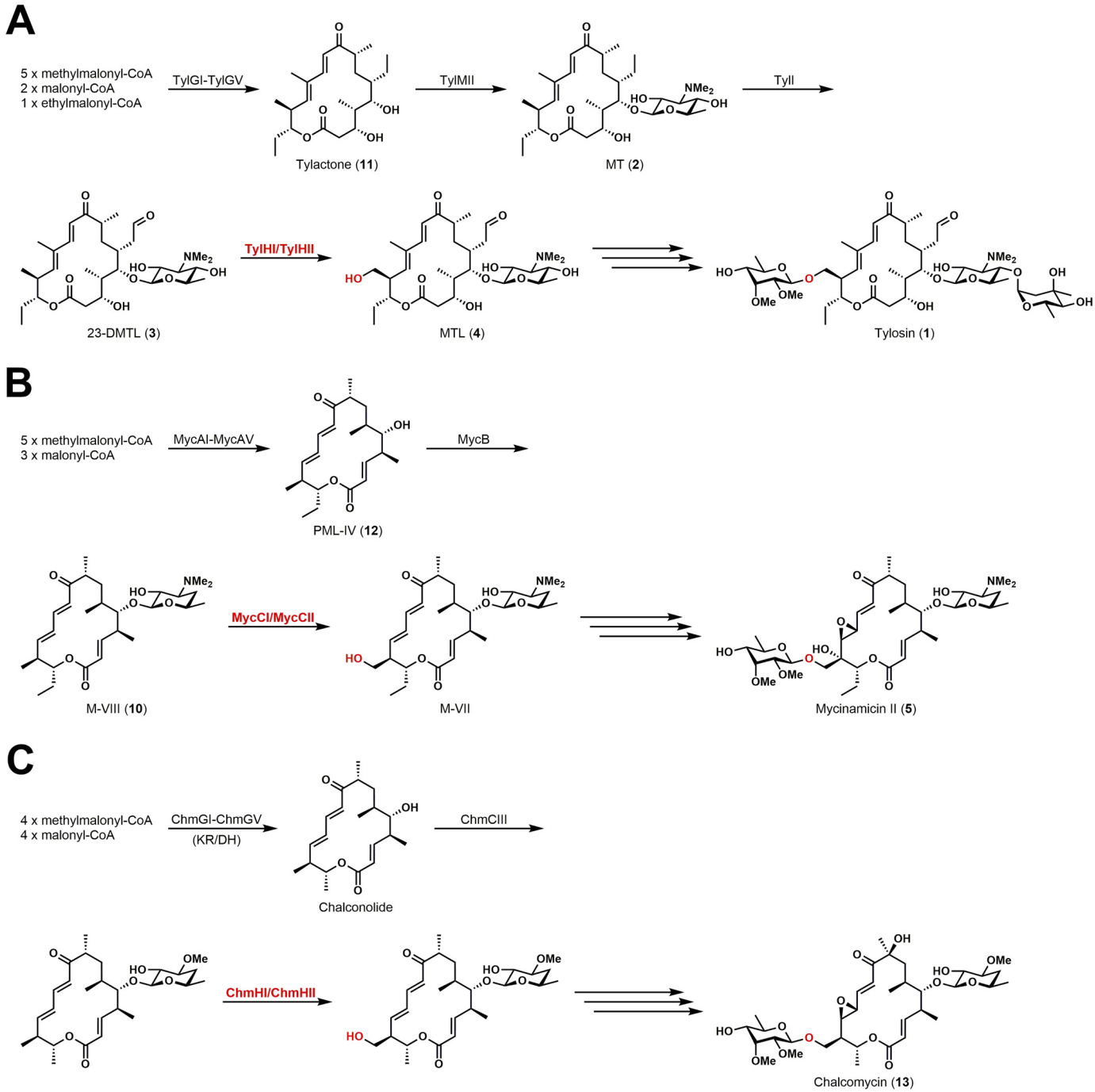

Scheme 1. Abbreviated biosynthetic pathways of representative 16-membered ring macrolides. Reactions catalyzed by P450/ferredoxin combinations described in this study are highlighted in *red*. *A*, tylosin (*tyl*) biosynthetic pathway in *S. fradiae*. *B*, mycinamicin (*myc*) biosynthetic pathway in *Micromonospora griseorubida*. *C*, chalcomycin (*chm*) biosynthetic pathway in *S. bikiniensis*.

ing to their bioactivity by performing late-stage oxidative tailoring reactions (12–17). Members of the CYP105 and CYP107 families are particularly well-represented among actinomycetes and include those with broad substrate scope (*e.g.* MoxA (CYP105AB3) (18, 19) and PikC (CYP107L1) (20)). Homologs of CYP105 have been identified in all *Streptomyces* species that have hitherto been investigated, with at least 17 subfamilies making up this P450 family in streptomycetes (21). These enzymes are chiefly involved in the metabolism of xenobiotics and in the biosynthesis of natural products, many of which are macrocyclic polyketides.

Tylosin (**1**) is a 16-membered ring macrolide antibiotic produced by several *Streptomyces* species, including *Streptomyces fradiae*, *Streptomyces rimosus*, and *Streptomyces hygroscopicus* (22–24). Although not used clinically in humans, it has been widely adopted in veterinary medicine as an antibacterial agent as well as in the livestock industry as a growth promoter. The biosynthesis of **1** in *S. fradiae* has been studied intensively over the past four decades (Scheme 1*A*) (25). Many of the steps in its assembly were initially elucidated in the early 1980s based on analysis of metabolites produced by blocked mutants (26) and cross-feeding studies (27–32). Only later were the genes asso-

ciated with the corresponding *tyl* biosynthetic gene cluster identified and sequenced (33, 34). The *tyl* cluster encodes two P450s whose functional roles were originally assigned by investigating the ability of *S. fradiae* cell-free extracts to oxidize various tylosin biosynthetic intermediates (30, 32). Recently, the activities of these two enzymes have been confirmed by our group through *in vitro* biochemical analysis (35, 36). TylI catalyzes a four-electron oxidation at C20 of 5-*O*-mycaminosyltylactone (MT; **2**) to produce 23-deoxy-5-*O*-mycaminosyl-tylonolide (23-DMTL; **3**), which TylHI then hydroxylates at C23 to give 5-*O*-mycaminosyl-tylonolide (MTL; **4**) (Scheme 1*A*). A third P450 gene (*orf16**) is also found in the *tyl* cluster, but it likely plays a role in the transcriptional regulatory cascade that controls tylosin production (37, 38).

Previously, we explored the substrate scope of MycCI (CYP105L2), a P450 from the related mycinamicin (**5**) pathway (Scheme 1*B*), and found that it is capable of hydroxylating a relatively broad range of 16-membered ring macrolactones and macrolides (35). However, parallel characterization of its close homolog TylHI (CYP105L1; 55% sequence identity) revealed that the latter is unable to tolerate even subtle changes to its native substrate. Differences in catalytic activity between P450 isozymes that are part of the same subfamily (≥55% identity) and that act on similar types of substrates have frequently been observed among mammalian P450s. Similar cases can be found among P450s involved in bacterial natural product biosynthesis. The P450 $OxyB_{van}$, which catalyzes the first oxidative phenolic coupling reaction in the biosynthesis of vancomycin, tolerates a number of nonnatural peptide substrates, whereas its homolog from the teicoplanin pathway ($OxyB_{tei}$; 74% sequence identity) exhibits a high degree of substrate selectivity (39). Moreover, whereas the P450s HmtT and HmtN involved in himastatin biosynthesis are 55% identical, they catalyze different types of reactions at unique sites on nearly identical substrates (40, 41). Drawing additional inspiration from these examples, we sought to acquire detailed insight into the molecular basis for substrate specificity in TylHI using a combination of biochemical, structural, and computational approaches. We aimed to use this information to understand the factors governing differences in the reactivity profiles of this selective enzyme and its relatively flexible homolog (MycCI). Rational design of functional TylHI/MycCI chimeras then allowed us to test the roles of specific regions of each P450 in mediating substrate binding and turnover, ultimately lending support to a more general model of P450/substrate interactions.

Results

TylHI activity and binding assays with substrate analogs

In our previous studies describing the catalytic versatility of MycCI, we found that its homolog TylHI possessed a comparatively restricted substrate scope (35). Whereas TylHI readily converted its native substrate (23-DMTL; **3**) to the expected product (MTL; **4**), minor alterations to the structure of this compound rendered it minimally reactive as a substrate for the enzyme. Specifically, an analog lacking the C20-aldehyde and the C4′-hydroxyl (5-*O*-desosaminyl-tylactone (DT); **6**) bound with nearly 500-fold lower affinity and was turned over less

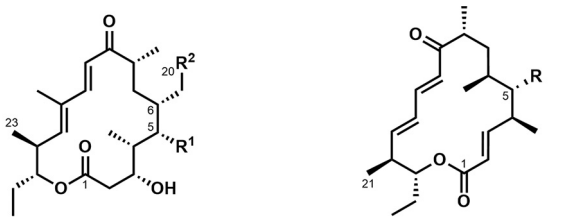

Compound	R^1	R^2
MT (**2**)	Mycaminose	CH_3
23-DMTL (**3**)	Mycaminose	CHO
20-OH-MT (**8**)	Mycaminose	CH_2OH
DT (**6**)	Desosamine	CH_3
23-DDTL (**7**)	Desosamine	CHO
20-OH-DT (**9**)	Desosamine	CH_2OH
Tylactone (**11**)	OH	CH_3

Compound	R
M-VIII (**10**)	Desosamine
PML-IV (**12**)	OH

Mycaminose: **R** = OH
Desosamine: **R** = H

Figure 1. Structures of macrocyclic substrates employed in this study.

than once (mol of product/mol of P450). Given the difference in only two functional groups between these two molecules, we questioned whether one might have a more significant impact on binding and subsequent catalysis than the other. Thus, we envisioned acquiring two additional substrate analogs via semisynthesis, one bearing the aldehyde and lacking the sugar hydroxyl group (23-deoxy-5-*O*-desosaminyl-tylonolide (23-DDTL); **7**) and another lacking the former but maintaining the latter (MT; **2**) (Fig. 1).

In our recent work detailing the chemoenzymatic total synthesis of tylactone-based macrolides, we reported the efficient *in vitro* TylI-catalyzed hydroxylation of **6** at C20 followed by selective chemical oxidation at the same site to give **7**, a biologically active macrolide called M-4365 G_2 (36). To access **2**, we followed a previously established scheme with some minor variations (Scheme S1). Reduction of the aldehyde of **3** with sodium borohydride followed by iodination of the alcohol (20-hydroxy-5-*O*-mycaminosyl-tylactone (20-OH-MT); **8**) and subsequent borohydride-mediated reduction afforded **2**. In addition to the target substrates, we opted to test the C20-hydroxylated synthetic intermediates **8** and 20-hydroxy-5-*O*-desosaminyl-tylactone (20-OH-DT; **9**) against TylHI in parallel activity assays.

Analytical-scale reactions with each substrate were performed with purified TylHI and maltose-binding protein–tagged spinach ferredoxin reductase (MBP-FdR) along with native ferredoxin TylHII or its homolog MycCII. The single-component TylHI-RhFRED fusion protein developed previously (35) was also tested in these assays. Although reduction of the aldehyde in the native substrate (**3**) to the alcohol (**8**) had no negative impact on conversion, further reduction to the alkane (**2**) resulted in a more substantial decrease in enzyme activity (88% conversion of **3** *versus* 40% conversion of **2** by TylHI/MycCII; see Fig. 2*A*). However, substitution of desosamine for mycaminose while maintaining the oxidation state of C20 had a more significant negative effect on substrate turnover (6% conversion of **7** by TylHI/MycCII). The same trend was observed for the other catalytic systems, with the native partnering of TylHI/TylHII somewhat tempering the damaging impact of substrate modification on activity and the artificial TylHI-RhFRED self-sufficient catalyst exacerbating it (Fig. 2*A*).

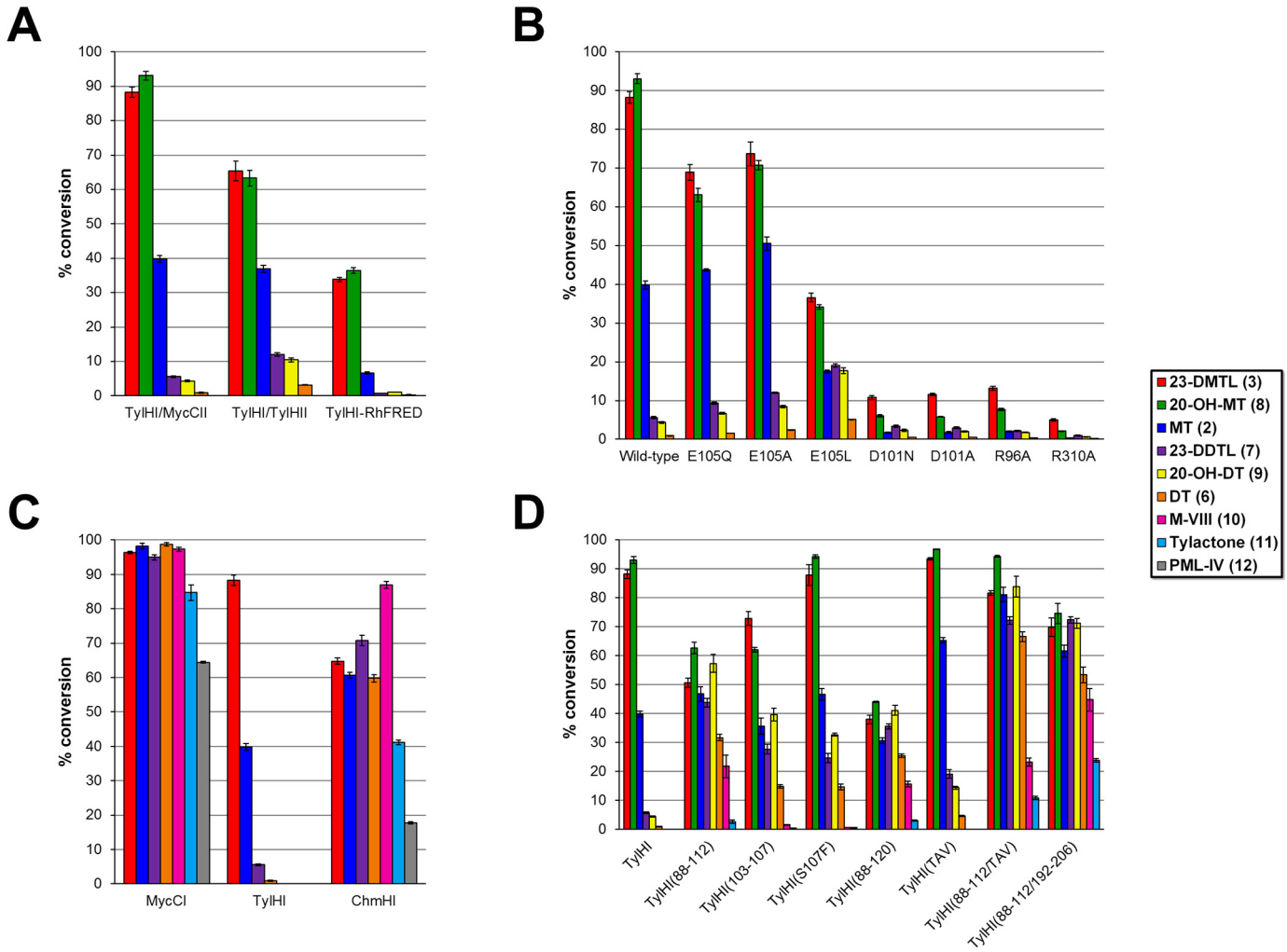

Figure 2. Results of activity assays employing different TylHI/redox partner combinations (*A*); selected TylHI mutants (*B*); MycCI, TylHI, and ChmHI (*C*); and selected TylHI/MycCI chimeras (*D*). Except for reactions employing TylHII and TylHI-RhFRED (labeled accordingly in *A*), all reactions were performed using MycCII and MBP-FdR as surrogate ferredoxin and ferredoxin reductase partners, respectively. *Bars* colored according to substrate indicate the mean of three independent experiments; associated *error bars* represent S.D. See Table S1 for raw numerical values and for the results of additional enzyme/substrate combinations.

To corroborate the results of the P450 functional assays, equilibrium substrate binding experiments were conducted (Table 1; see Table S2 for relative fractional spin shifts and Fig. S7 for representative binding plots). Generally, the binding affinities of the substrates tested were consistent with the degrees to which they were converted to their respective products. Reduction of the aldehyde in **3** to the alcohol (**8**) modestly increased the K_d from 0.63 to 4.3 μM, and further reduction to the alkane (**2**) had a more significant impact on binding (K_d = 45 μM). Mirroring the effect of removing the C4′-hydroxyl group on substrate turnover, the K_d for binding of **7** to TylHI (236 μM) was 375-fold higher than that for binding of **3**. Although turnover of the other desosaminylated substrates (**6** and **9**) was lower compared with **7**, they bound with about the same affinities to TylHI.

Taken together, these data obtained with key analogs of the native substrate (**3**) have revealed that, independent of the oxidation state of C20, compounds with mycaminose as the deoxyamino sugar are strongly preferred over those bearing desosamine. Although TylHI preferentially accepts substrates with an oxidized C6 ethyl side chain, the presence or absence of a hydroxyl group attached to C4′ of the sugar has a much more significant impact on substrate binding and subsequent turnover.

Structural characterization of TylHI bound to 23-DMTL

To acquire new insights into the specific interactions involved in TylHI substrate binding, we solved the crystal structure of the enzyme in complex with its native substrate 23-DMTL (**3**) to a resolution of 1.99 Å (Table 2). The asymmetric unit of the crystal lattice contains two protein molecules, and in each case, electron density for the first 31 amino acids is not observed. Alignment of the primary amino acid sequence of TylHI with that of MycCI reveals that the latter starts at residue 32 of TylHI (see Fig. 7). To probe any potential role for this N-terminal portion of the TylHI sequence, the corresponding N-terminal truncated protein ($TylHI_{\Delta 2-33}$) was generated and tested in parallel with the WT enzyme. No significant differences in activity or protein stability were observed, raising the possibility that the N-terminal sequence

Table 1
Dissociation constants of selected substrates against wildtype TylHI
Reported errors are those obtained from fitting data averaged from experiments performed in duplicate.

Substrate	K_d
	μM
2	45 ± 3
3	0.63 ± 0.02
8	4.3 ± 0.4
6	210 ± 8
7	236 ± 23
9	235 ± 17

may function in some unknown capacity in the host organism (see Table S1 for results of activity assays employing $TylHI_{\Delta 2-33}$).

The two chains in the asymmetric unit exhibit minimal conformational ambiguity (root mean square deviation, 0.26 Å). However, a few minor differences between chains A and B can be discerned. Notably, although **3** is bound in both monomers, the C6-ethyl aldehyde moiety adopts two different orientations relative to the rest of the macrocycle in chain A (Fig. 3*A*). Three water molecules overlap between the two chains, only one of which, located near the surface of the protein, is poised to interact directly with **3** via polar groups on the mycaminose sugar (Fig. 3*A*).

TylHI exhibits an overall tertiary structure very similar to that of MycCI (root mean square deviation, 0.76 Å; Fig. S1, *A* and *B*) and many other P450 enzymes. Moreover, like the binding pocket of MycCI, that of TylHI is highly hydrophobic and accommodates the macrocyclic substrate bound diagonally above the distal face of the heme cofactor (Fig. 3). The primary methyl group (C23) is located within 3.8 Å of the heme iron center, and its orientation relative to the cofactor is consistent with the experimentally observed site of hydroxylation.

As observed in MycCI, the base of the substrate proximal to the heme in TylHI is surrounded by six hydrophobic residues (Leu-111, Leu-255, Ala-259, Ala-306, Leu-309, and Val-410) that help to position it in the proper orientation for activation of the target C–H bond. With the exception of Val-410 (Ile-378 in MycCI), these residues are identical to those found in MycCI and are located in the same relative positions (Fig. 3). Other amino acid side chains that form part of the hydrophobic wall of the binding pocket near the I helix (*e.g.* Ala-195, Leu-208, Leu-211, Val-254, and Ala-258) are also identical to those present in MycCI. Despite these similarities between the two proteins, key differences are readily apparent, including the identity and relative positioning of several residues in the BC and FG loop regions. Although more than half of the residues that comprise the BC loop are conserved between MycCI and TylHI and many of the substitutions are relatively conservative, differences in the positions of several side chains that reflect deviations in the Cα backbone are evident. One particular region in the middle of the TylHI BC loop contains residues that closely approach bound **3** (Ser-100–Ala-106) as well as those whose positions are displaced relative to the homologous residues in MycCI (Arg-96, Glu-103, Glu-105, Ser-107, and Arg-108 in TylHI corresponding to Arg-65, Asp-72, Asp-74, Phe-76, and Arg-77 in MycCI; Figs. 4, 6, S1*D*, and S2).

Additional differences in amino acid composition and positioning are observed in the FG loop and N-terminal portion of the G helix, most markedly in substitutions of small residues (Ala-199 and Ala-200 in TylHI) for larger polar/charged residues (Asn-168 and Asp-169 in MycCI), insertion of a glycine (Gly-201 in TylHI with no counterpart in MycCI), and charge reversal (Glu-203 in TylHI in place of Arg-171 in MycCI). However, the side chains of these amino acids do not appear to directly interact with bound substrate in either structure, and the overall fold of the region is unperturbed.

Table 2
Crystallographic data summary for TylHI/23-DMTL
AU, asymmetric unit; r.m.s., root mean square.

Crystal data	
Protein	TylHI
Ligand	23-DMTL
PDB code	6B11
Data collection	
Space group	$P2_12_12_1$
Cell dimensions	
a, *b*, *c* (Å)	63.7, 109.2, 150.1
α, β, γ (°)	90.0, 90.0, 90.0
Molecules in AU	2
Wavelength (Å)	1.11587
Resolution (Å)	1.99
R_{sym} or R_{merge} (%)	7.0 (174.0)[a]
$I/\sigma I$	14.6 (1.39)
Completeness (%)	95.6 (69.7)
Redundancy	6.2 (3.2)
Refinement	
No. reflections	66,461
R_{work}/R_{free} (%)	19.4/24.0
No. atoms	
Protein	5,907
Heme	86
Substrate	123
Solvent	234
Mean B value	46.5
B-factors	
Protein	47.0
Heme	36.9
Substrate	38.6
Solvent	49.3
r.m.s. deviations	
Bond lengths (Å)	0.019
Bond angles (°)	1.966

[a] Values in parentheses are for the highest resolution shell.

The mycaminose-binding pocket is composed of residues that are mostly found in the BC and FG loops of TylHI. These residues are typically more polar than those comprising the binding pocket for the rest of the macrocycle. A salt bridge network involving Arg-96, Asp-101, Glu-105, and Arg-310 surrounds one side of the substrate proximal to the sugar (Figs. 4*A* and S2*A*). Despite the presence of similar residues in MycCI (Arg-65, Asp-70, Asp-74, and Arg-278), they do not all interact to form a cohesive network around the desosamine unit of mycinamicin VIII (M-VIII; **10**) (Figs. 4*B* and S2*B*). Although the Asp-70–Arg-278 interaction is present in MycCI, Arg-65 and Asp-74 are completely displaced out of the pocket and exposed to bulk solvent.

Specific polar interactions between TylHI and **3** are confined to the aldehyde substituent and portions of the deoxyamino sugar (Fig. 4*A*). In chain A, the electron density surrounding the C6-ethyl aldehyde moiety suggests that this part of the substrate adopts two different conformations when bound to TylHI (Fig. S3). In the particular conformation closer to that observed in chain B, the carbonyl of the aldehyde is poised to accept a hydrogen bond from the side chain of Glu-105 in its protonated form and/or from a neighboring water molecule.

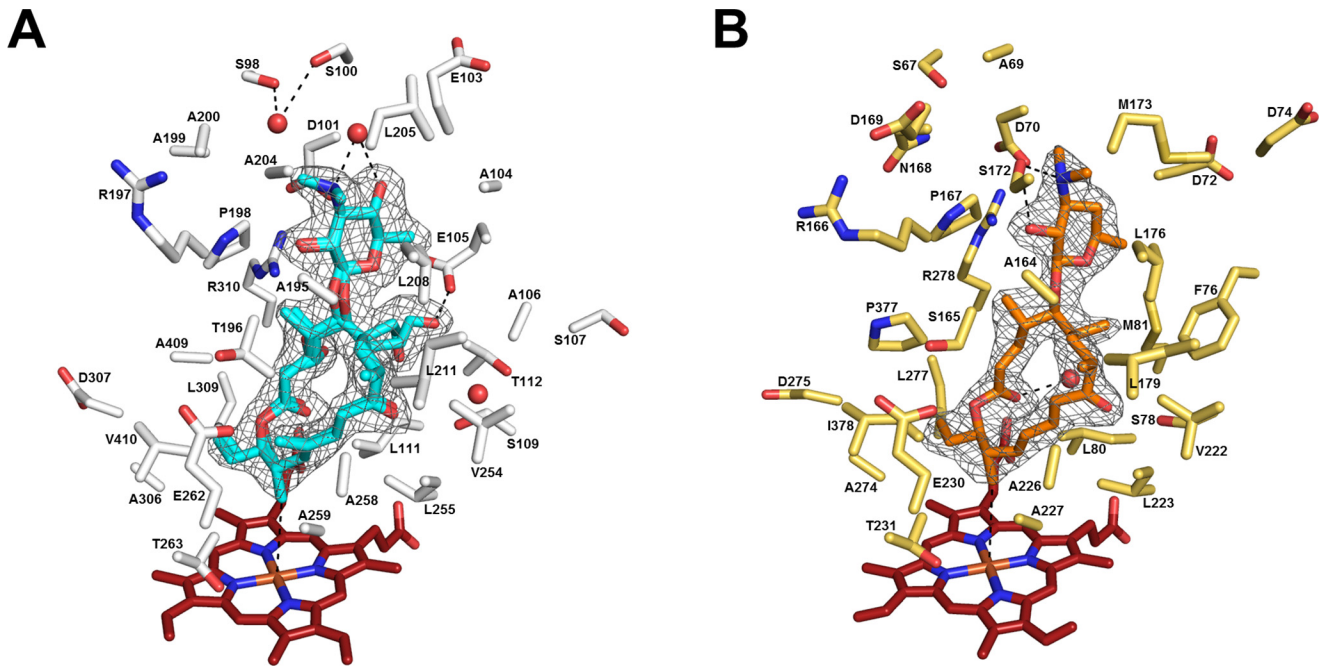

Figure 3. Comparison of the crystal structures of TylHI (PDB code 6B11) and MycCI (PDB code 5FOI) bound to 3 and 10, respectively. *A*, binding pocket of **3** in TylHI. The substrate (**3**) is depicted in *cyan*, the heme cofactor is shown in *firebrick*, and the side chains of residues within 5 Å of **3** are *white* and labeled accordingly. *Gray mesh* surrounding **3** represents the $F_o - F_c$ omit map (generated by setting the occupancy of substrate to zero) contoured at 3 σ. The three water molecules present in both chains of the asymmetric unit are shown as *small red spheres*. Potential hydrogen bonding interactions are depicted as *black dashes*. A *black dash* is also drawn between the heme iron and the carbon atom (C23) targeted for hydroxylation. *B*, binding pocket of **10** in MycCI shown in the same relative orientation as that of **3** in TylHI. The substrate (**10**) is depicted in *orange*, the heme cofactor is shown in *firebrick*, and the side chains of residues within 5 Å of **10** are *yellow–orange* and labeled accordingly. *Gray mesh* surrounding **10** represents the $F_o - F_c$ omit map (generated by setting the occupancy of substrate to zero) contoured at 3 σ. The single water molecule present in both chains of the asymmetric unit is shown as a *small red sphere*. Potential hydrogen bonding interactions are depicted as *black dashes*. A *black dash* is also drawn between the heme iron and the carbon atom (C21) targeted for hydroxylation.

Two additional direct polar interactions between TylHI and bound **3** are localized to the mycaminose substituent (Figs. 4*A* and S2*A*). As observed in the MycCI/**10** structure (Figs. 4*B* and S2*B*), the C2′-hydroxyl group of the sugar donates a hydrogen bond to the backbone carbonyl of Ala-195 (Ala-164 in MycCI). Furthermore, the C4′-hydroxyl appended to mycaminose interacts with the backbone amide nitrogen and carbonyl oxygen atoms of Gly-102 and Glu-103 in TylHI, respectively (Fig. 4*A*). On the basis of the results of activity and binding assays with substrate analogs (see above), these polar interactions appear to be critical for substrate recognition in TylHI. Indeed, the simple removal of the C4′-hydroxyl of mycaminose results in a drastic reduction in binding affinity and a concomitant decrease in substrate conversion.

It is also important to note that no direct interactions with the C3′-nitrogen of mycaminose are observed in either chain of the crystal structure. The carboxylate of Asp-101 in TylHI is located ~5 Å away from this position on the deoxyamino sugar, which is not close enough to provide a salt bridge contact. In addition, because the negative charge of the Asp-101 side chain is probably neutralized via interactions with Arg-96 and Arg-310, it likely plays a minimal role in compensating for the positive charge of the protonated tertiary amine.

Analysis of TylHI site-directed mutants

Analysis of the TylHI/**3** cocrystal structure provided key insights into the molecular basis for substrate recognition, highlighting several notable differences from the homologous MycCI/**10** system. To validate and further probe the roles of certain amino acid residues in substrate binding, several mutants were generated and tested against the panel of six compounds described previously (Fig. 1). The results of the activity and binding assays with **2** demonstrated that the aldehyde portion of the native substrate (**3**) does not provide a critical recognition element for TylHI. Although the side chain of Glu-105 is positioned to interact with the aldehyde in the crystal structure, the ambiguity surrounding the protonation state of the former as well as the conformation of the latter made it difficult to assign a definitive role for this residue.

As expected, only modest reductions in activity were observed for the E105Q and E105A mutants acting on **3** (69–74% conversion for the mutants *versus* 88% conversion for WT) and its reduced analog **8** (Fig. 2*B*). However, activity marginally increased across the various other substrates tested. The E105L mutant was generated to control for any potential decrease in activity resulting from disruption of key van der Waals interactions that could be stabilizing this region of the protein. Interestingly, although activity on the mycaminosylated substrates (**2**, **3**, and **8**) decreased relative to the WT enzyme (*e.g.* 37% conversion of **3**), the E105L mutation enabled TylHI to more effectively hydroxylate the desosaminylated substrates (**6**, **7**, and **9**; ~3–6-fold increased conversion compared with the WT enzyme; Fig. 2*B*). The loss of a negative charge and concomitant addition of a methyl group to the side chain of the target residue likely increased the hydrophobicity of the binding pocket, lead-

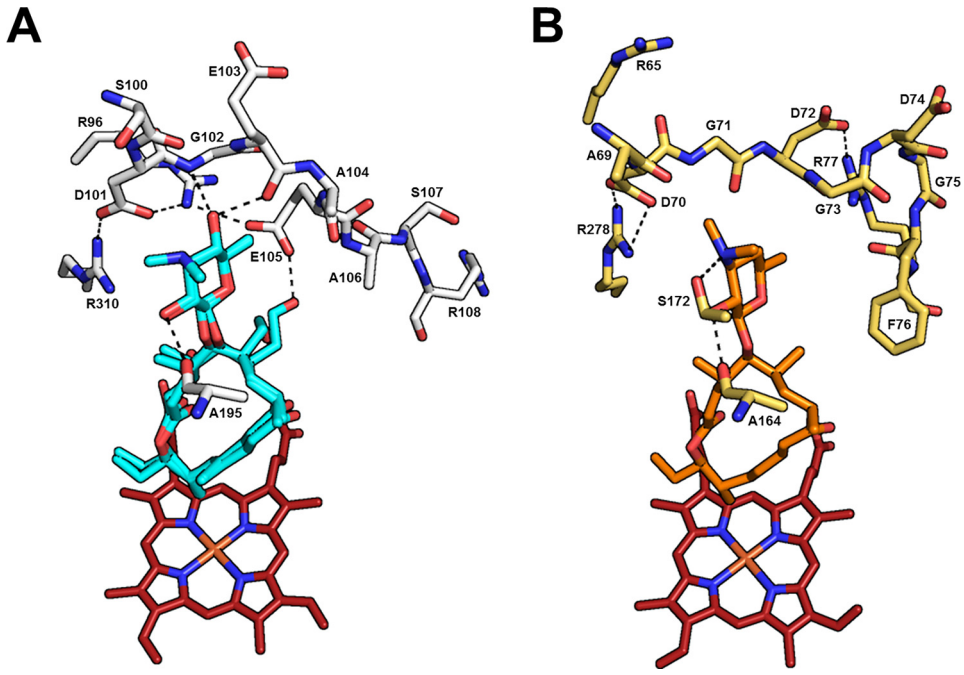

Figure 4. Comparison of substrate contacts and other key interactions in the active sites of TylHI (*A*) and MycCI (*B*). Substrates and amino acid residues are colored as in Fig. 3. Main-chain atoms are depicted for residues Ser-100–Arg-108 and Ala-195 in TylHI and for residues Ala-69–Arg-77 and Ala-164 in MycCI. *Black dashes* are drawn between atoms involved in potential polar contacts. For improved clarity, water molecules have been omitted. See Fig. S2 for alternative viewing angles.

ing to better binding of suboptimal substrates bearing desosamine (Table S2).

Consistent with the results of the activity assays, relatively minor decreases in affinity were associated with the binding of **3** to the E105Q and E105A mutants (Table 3). Interestingly, although **3** bound >100-fold more weakly to the E105L mutant than to the WT enzyme, desosaminylated analog **7** bound twice as tightly, thus explaining the enhanced turnover of this compound by this particular mutant (19% conversion for $TylHI_{E105L}$ *versus* 6% conversion for the WT enzyme).

Additional mutagenesis targets consisted of several charged residues in the BC loop forming part of the mycaminose-binding pocket. One residue (Asp-101) was found in proximity to the *N*,*N*-dimethylamino group of the sugar, potentially helping to neutralize the positive charge associated with the protonated tertiary amine. Both the D101N and D101A mutants exhibited substantial losses in activity across all substrates tested, with conversion of **3** diminishing to 11–12% and that of the other substrates falling at or below 6% (Fig. 2*B*). Binding of **3** was substantially weakened as well, with K_d values even higher than those observed for binding of the desosaminylated substrates to the WT enzyme (Table 3). Nonetheless, these data alone were not enough to gain a complete understanding of the specific role of this residue in mediating substrate binding.

Because Asp-101 is located in the middle of a salt bridge network involving Arg-96 and Arg-310 (Fig. 4*A*), the latter two residues were subsequently targeted for mutagenesis to explore whether disruption of the network could be used to rationalize attenuated substrate binding and turnover. Each of the corresponding arginine-to-alanine mutants showed a loss in catalytic activity that was comparable to that observed for the Asp-101 mutants; R310A exhibited the most dramatic effect, with conversion of **3** under standard reaction conditions dropping to 5% (Fig. 2*B*). The R96A and R310A mutants also had dissociation constants with respect to **3** that were similar to those for the Asp-101 mutants (Table 3). Incidentally, the K_d values for binding of **3** to all of these mutants approached that for binding of the corresponding aglycone (tylactone; **11**) to the WT enzyme (K_d = 282 μM; see Table S2).

Taken together, these results are consistent with the key role of salt bridge contacts among Arg-96, Asp-101, and Arg-310 in facilitating the formation of a binding pocket for the deoxyamino sugar moiety of the substrate. Although this triad of charged residues is identical between TylHI and MycCI, only one salt bridge is preserved (Asp-101–Arg-310 in TylHI, corresponding to Asp-70–Arg-278 in MycCI). However, in contrast to the drastic loss in activity that TylHI incurred upon mutation of Asp-101, no such impact was observed for Asp-70 mutants of MycCI (Table S1). However, because MycCI is somehow equipped to effectively bind substrates without deoxyamino sugars, any disruption of the binding pocket proximal to the sugar is likely to have a relatively insignificant effect on substrate turnover.

Molecular dynamics simulations of TylHI and MycCI

The results of biochemical experiments employing substrate analogs as well as the details of the crystal structure and functional effects of site-directed mutations described thus far had provided some important insights into the molecular basis for substrate recognition in TylHI and enriched our understanding of it as a highly specific enzyme compared with MycCI. However, understanding why MycCI could bind and hydroxylate both mycinamicin- and tylosin-type substrates, whereas TylHI only showed appreciable activity on mycaminosylated versions

Table 3
Dissociation constants of 23-DMTL (3) and 23-DDTL (7) against TylHI mutants
K_d values are shown in μM. Reported errors are those obtained from fitting data averaged from experiments performed in duplicate.

TylHI mutant	3	7
Wildtype	0.63 ± 0.02	236 ± 23
E105Q	11 ± 1	245 ± 14
E105A	5.1 ± 0.3	200 ± 17
E105L	69 ± 4	118 ± 10
D101N	281 ± 12	ND[a]
D101A	263 ± 22	ND
R96A	175 ± 11	ND
R310A	249 ± 15	ND

[a] ND, value not determined.

of the latter, remained elusive. In an effort to further understand the molecular-level details giving rise to this observation, we performed molecular dynamics (MD) simulations on each enzyme using both **3** and **10** as probe substrates. In the present study, and consistent with previous experimental results (35), MycCI exhibited near complete conversion of both **3** and **10**, whereas TylHI was only active on **3** (Table S1). Moreover, whereas MycCI had been shown to bind these compounds in the low nanomolar range (35), TylHI bound **3** and **10** with K_d values near 1 μM and 1 mM, respectively (Table S2).

In initial MD simulations, the distance from the carbon atom of the methyl group targeted for oxidation in each compound (C23 for **3**; C21 for **10**) to the oxygen atom of the modeled Compound I iron–oxo species was monitored over a 500-ns trajectory (Fig. 5*A*). For MycCI, the average distances for both compounds were 3.0–3.5 Å. In contrast, whereas C23 of **3** occupied a similar range of distances away from the iron–oxo species of TylHI over the course of the simulation, the distance increased up to 5–6 Å for the corresponding C21 of **10**. These results are consistent with the experimental data and serve to highlight the inherent incompatibility of **10** with the TylHI active site.

Next, the relative strengths of the hydrogen bonds between the C4′-hydroxyl group appended to the mycaminosyl moiety of **3** and the backbone amide nitrogen and carbonyl oxygen atoms of Gly-102 and Glu-103 were examined. The results of the 500-ns MD simulation demonstrated that these hydrogen bonds are stable, with that formed between the substrate and the carbonyl oxygen atom of Glu-103 maintained at an average distance of 1.9 Å throughout the simulation and thus appearing to be the strongest among the three tested (Fig. 5*B*). Although it is unlikely that the strengths of these interactions are alone sufficient to promote such tight binding of **3** (K_d = 0.63 μM) relative to **7** (K_d = 236 μM) lacking a C4′-hydroxyl group, their presence may be important for overall stabilization of the salt bridge network between Arg-310 and some of the key charged residues in and around the BC loop.

As noted previously, close inspection of the TylHI and MycCI crystal structures reveals that the BC loops, which surround and partially cover the bound substrate in each case, are different in several respects between the two enzymes (Figs. 4 and 6). In MycCI, charged residues in the BC loop and N-terminal portion of the C helix appear to form a more robust salt bridge network with the potential for more intraprotein interactions in this region of the enzyme (Fig. 6*B*). A less elaborate network is observed for TylHI (Fig. 6*A*). MD simulations were used to characterize the relative strengths of these salt bridges by monitoring the distances between oppositely charged residues over time. The results demonstrated that, although the salt bridge networks are qualitatively different between MycCI and TylHI, they are stable and likely maintained in both enzymes. Heat maps (Fig. 6) depict the strength of individual interactions in the network in terms of the inverse of the average distance between each pair of residues engaged in a salt bridge. Clearly, there are more nodes in the network and more salt bridge interactions in MycCI compared with TylHI. We hypothesize that the relative weakness of the TylHI salt bridge network may contribute to its unusual sensitivity to substrate structure and could explain the severely attenuated binding affinities toward tylosin-type substrates bearing desosamine.

Overall, the insights gained from this computational investigation are consistent with the experimental data described previously. In TylHI, nodes in the salt bridge network that appear to be most critical for effective substrate binding include those involving Asp-101, Arg-96, and Arg-310. However, although Glu-105 appears to maintain a stable salt bridge with Arg-96 throughout the MD simulation, the E105Q and E105A mutations had minimal effects on TylHI substrate binding and catalytic activity (see above). For MycCI, although a stable salt bridge is maintained between Asp-70 and Arg-278, the D70N and D70A mutants exhibited virtually no loss in catalytic activity across each of the substrates tested (Table S1). In addition to Asp-70, Arg-77 appears to lie at the center of another important region of the salt bridge network in MycCI. Interestingly, although the R77A mutant showed >90% conversion of each of the macrolide substrates, its ability to hydroxylate the aglycones tylactone (**11**) and PML-IV (**12**) was diminished (Table S1). This result suggests that the salt bridge interactions established between Arg-77 and other residues in the BC loop may play roles in facilitating macrolactone binding.

Comparative analysis of the TylHI/MycCI homolog ChmHI

To provide further insight into the divergent substrate specificity of TylHI and MycCI, we identified ChmHI as a close homolog of both enzymes and tested its activity across the same panel of macrolactone and macrolide substrates. This P450 is thought to play an analogous role in the biosynthesis of the macrolide chalcomycin (**13**) in *Streptomyces bikiniensis* (Scheme 1*C*) (42). Interestingly, multiple-sequence alignment of the three homologous P450s reveals that ChmHI is roughly equally similar to both MycCI (62% identity) and TylHI (57% identity), with regions of identity and divergence scattered throughout the sequence (Fig. 7). In addition, as for MycCI and TylHI, the gene encoding ChmHI is located adjacent to one that encodes a small [3Fe-4S]-type ferredoxin protein, ChmHII. Therefore, ChmHI paired with either ChmHII or the native MycCI ferredoxin (MycCII) was tested in parallel with the catalytically self-sufficient ChmHI-RhFRED fusion protein as well as MycCI and TylHI against various macrolactone and macrolide substrates.

Despite the absence of its purported native substrate from the panel, the functional activity of ChmHI was verified by its ability to convert each of the substrates tested to products with

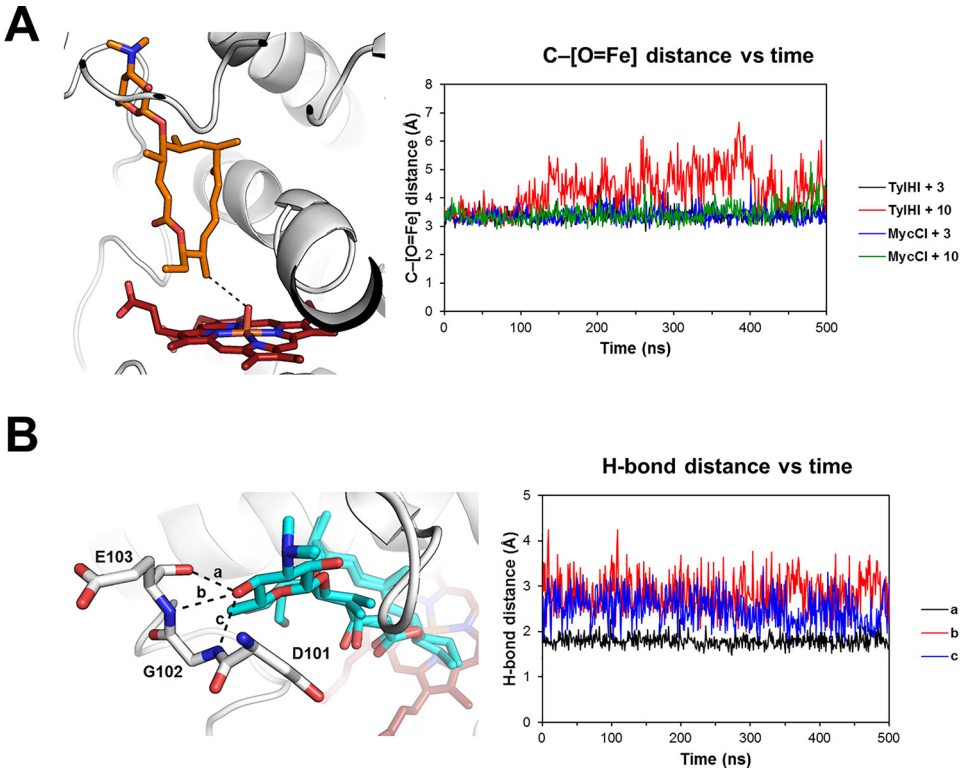

Figure 5. MD simulations performed on TylHI and MycCI. *A*, C–[O=Fe] distance as a function of time (500-ns trajectories) for TylHI and MycCI in complex with either substrate **3** (23-DMTL) or substrate **10** (M-VIII). The initial binding pose of **10** in MycCI was acquired from the crystal structure (PDB code 5FOI), whereas those for the remaining substrate/enzyme complexes were obtained from computational docking. In all cases, the heme was modified to the iron–oxo (Fe=O) intermediate. The image to the *left* of the MD traces shows the initial binding pose of **10** (*orange*) in TylHI (*white*). *B*, hydrogen bonding interactions observed between the backbone amide nitrogen and carbonyl oxygen atoms of Gly-102 and Glu-103 and the C4′-hydroxyl group of **3** (*cyan*) in the TylHI crystal structure. The distances of three H-bonds (*a*, *b*, and *c*) were monitored over a 500-ns trajectory.

the same retention times as those of the corresponding MycCI and TylHI reactions, indicating that this P450 has a broad substrate scope similar to MycCI (Fig. 2*C*). As observed for TylHI, the overall activity of ChmHI was highest when it was partnered with MycCII instead of its native ChmHII (Table S1), a result that was unsurprising given that the latter was found to suffer from some of the same expression and stability problems as TylHII. Curiously, ChmHI-RhFRED exhibited markedly low hydroxylation activity relative to the three-component catalytic systems across all substrates (Table S1). Subsequent LC-MS analysis of the ChmHI-RhFRED reaction mixtures demonstrated that *N*-demethylation constituted a significant portion of the product profile for reactions involving glycosylated substrates **6** and **10** (Table S3 and Fig. S4).

With these results in hand, we closely compared the sequences of each P450 to find any regions of similarity between MycCI and ChmHI as well as regions of divergence from TylHI (Fig. 7). We envisioned that identifying these regions and mapping them onto the structures of MycCI and TylHI could yield some important clues regarding the sequence determinants for the differences in substrate scope between these enzymes. Only seven of the 64 residues that are identical between MycCI and ChmHI but different from TylHI are located near bound substrate. Among these seven, four form a near-contiguous stretch in the middle of the BC loop, whereas the other three stand alone in the F/G helices and the C-terminal loop region comprising substrate recognition site 6 (SRS6) (43). Although the differences in the physical and chemical properties of these residues between MycCI/ChmHI and TylHI are minimal, examination of the MycCI and TylHI crystal structures reveals that the relative positions and conformations of the amino acids in the BC loop are quite different (Figs. 4 and 6).

Functional analysis of TylHI/MycCI chimeras

On the basis of our combined experimental and computational data, we set out to generate TylHI/MycCI chimeras to probe the role that different regions in each protein play in affecting substrate specificity for these enzymes. First, we constructed TylHI/MycCI BC loop chimeras to acquire a better understanding of the role of this particular structural element in influencing the notable differences in substrate specificity between these two proteins. In each of these enzymes, the BC loop consists of 32 residues, 15 of which vary between the two (Fig. 7). In the first set of experiments, the entire BC loop region of TylHI (residues 88–112) was replaced with that of MycCI, and the resulting chimera (designated $TylHI_{88-112}$) was expressed, purified, and tested against several tylosin- and mycinamicin-type 16-membered ring substrates. Remarkably, the chimera was able to convert all of the macrolide substrates to the appropriate monohydroxylated products, standing in stark contrast to the inability of WT TylHI to readily accept macrolides beyond those bearing mycaminose as the pendant deoxyamino sugar (Fig. 2*D*). Notably, although conversion of the native substrate **3** and its reduced analog **8** decreased, $TylHI_{88-112}$ turned over desosaminylated substrates (**6**, **7**, and

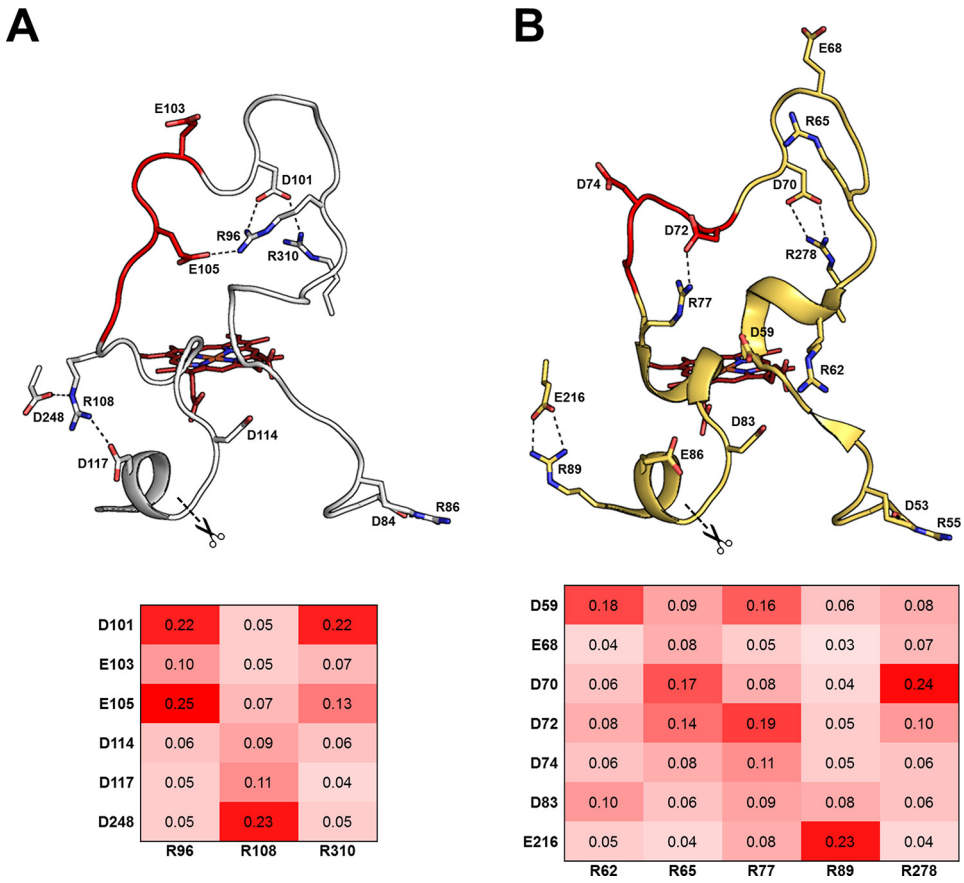

Figure 6. Comparison of key salt bridge interactions among residues in the BC loops of TylHI (*A*) and MycCI (*B*). Main chains and amino acid residues are colored as in Fig. 3. The entire region displayed as a contiguous stretch of residues (full BC loop + N-terminal portion of the C helix) corresponds to Asp-84–Ala-120 in TylHI and Asp-53–Arg-89 in MycCI. Key interactions are depicted as *black dashes*. In each case, two additional residues that reside outside the BC loop/C helix are shown (TylHI: Asp-248 and Arg-310; MycCI: Glu-216 and Arg-278). A pair of *scissors* adjacent to a *dashed line* marks the end of the BC loop and the beginning of the C helix in each structure. Residues Glu-103–Ser-107 in TylHI and Asp-72–Phe-76 in MycCI are highlighted in *red*. Heat maps below each structure report the relative strength of each salt bridge interaction as the inverse of the average distance (Å) between two given residues during the 500-ns MD simulation.

9) with comparable efficiency to mycaminosylated substrates (**2**, **3**, and **8**). Moreover, whereas TylHI could scarcely bind the native substrate for MycCI (**10**; K_d = 925 μM), the chimera exhibited appreciable activity on this compound (22% conversion). It also displayed a low-level ability to hydroxylate the aglycone **11** (3% conversion), but it showed no activity on **12**. Subsequent substrate titration experiments demonstrated that all of the macrolides investigated bound with similar affinities to this BC loop chimera (K_d = 16–41 μM; Table 4). Although the binding affinity for **3** decreased considerably for the chimera relative to the WT enzyme, it markedly improved for **2**, **6**, **7**, and **10**, with the latter mycinamicin-type substrate actually binding with the highest affinity among the macrolides tested (K_d = 16 μM). Interestingly, **11** bound only slightly more tightly to TylHI$_{88-112}$ than to WT TylHI despite the ability of the former to hydroxylate this substrate.

Encouraged by these results, we decided to further investigate a smaller portion of the BC loop identified previously as containing four residues proximal to bound substrate that are shared by MycCI and ChmHI but not maintained in TylHI (Fig. 6 shows this portion highlighted in *red* in the structures; see also Fig. S1*D*). Thus, the following amino acid substitutions were simultaneously introduced to TylHI, generating a chimera designated TylHI$_{103-107}$: E103D, A104G, E105D, A106G, and S107F. The purified protein was roughly intermediate between WT TylHI and TylHI$_{88-112}$ in terms of overall activity across the substrates tested (Fig. 2*D*). Whereas relatively modest decreases in conversion were observed for mycaminosylated compounds (**2**, **3**, and **8**), TylHI$_{103-107}$ was still considerably more active than WT TylHI on those bearing desosamine (**6**, **7**, and **9**). However, it did not turn over these substrates to the same extent as TylHI$_{88-112}$, and its activity on **10** and **11** was more substantially diminished. The results of experiments with TylHI$_{103-107}$ demonstrated that this particular region of the BC loop plays an important role in controlling the preference for the enzyme to bind mycaminosylated *versus* desosaminylated substrates. This finding becomes more apparent upon analysis of the binding data, which show that **6** and **7** bind with even higher affinities to TylHI$_{103-107}$ than to TylHI$_{88-112}$, representing substantial decreases in K_d values relative to WT TylHI (Table 4).

Next, we further probed residues 103–107 in TylHI$_{103-107}$ to determine the relative contribution of the individual amino acid changes in this chimera toward enhancing the binding of desosaminylated macrolides. Most notably, we found that the single mutant TylHI$_{S107F}$ was capable of hydroxylating substrates **6**, **7**, and **9** nearly as well as TylHI$_{103-107}$ without incurring any loss in activity toward substrates **2**, **3**, and **8** relative to

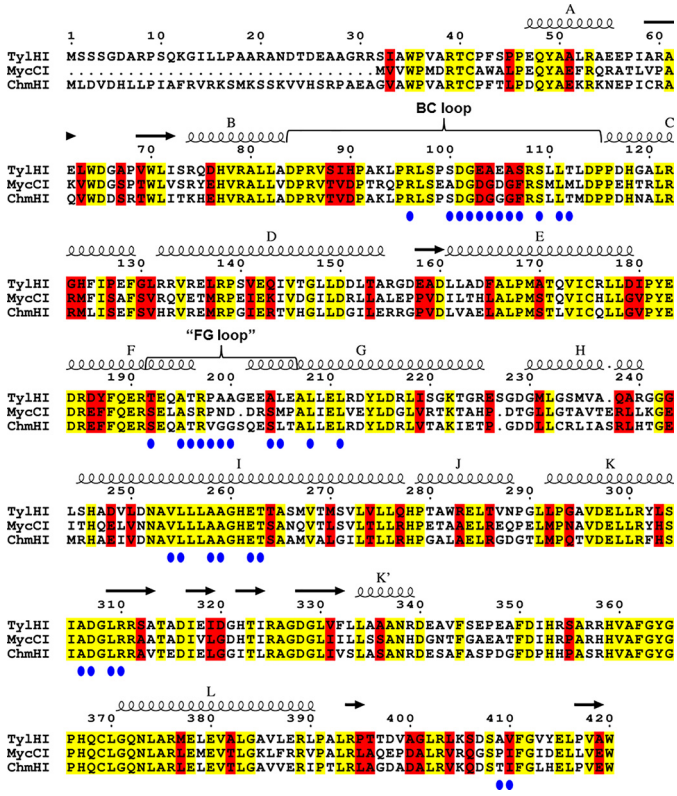

Figure 7. Multiple sequence alignment of TylHI, MycCI, and ChmHI. *Numbers* refer to the positions of residues in the TylHI sequence. Conserved secondary structural elements (α-helices (coils labeled *A–L*) and β-strands (*unlabeled arrows*)) based on the structures of MycCI and TylHI are depicted above the sequences. Residues highlighted in *yellow* are identical across all three proteins. Residues highlighted in *red* are identical or similar between MycCI and ChmHI but divergent from TylHI. *Blue circles* are located below residues found within 5 Å of bound substrate in the MycCI and TylHI crystal structures. The alignment was rendered using the ESPript 3.0 server (57).

WT TylHI (Fig. 2*D*). This result was corroborated by the equilibrium substrate binding data, which revealed large improvements over WT affinities across all substrates tested (Table 4). Although substitution of only a few amino acid residues (103–107, with S107F playing a predominant role) considerably attenuated the ability of TylHI to discriminate substrates solely on the basis of sugar identity, replacement of the entire BC loop (residues 88–112) was required for conferring on TylHI the ability to accept substrates possessing a different type of macrolactone scaffold (*i.e.* mycinamicin-type as in **10**).

The computational work described previously involved detailed analysis of some key salt bridge interactions between charged residues in and around the BC loop. We focused our attention on the salt bridges formed between Arg-77 and Asp-72 and between Arg-89 and Glu-216 in MycCI as well as between Arg-108 and Asp-248 in TylHI, all of which appear to be relatively strong on the basis of the MD simulations. Although Arg-77 in MycCI corresponds to Arg-108 in TylHI, their positions with respect to the rest of the BC loop differ considerably (Fig. 6). We hypothesized that the presence of an additional arginine residue at the N-terminal portion of the C helix in MycCI (Arg-89) may prevent Arg-77 from pointing down toward the C helix in a manner similar to the corresponding Arg-108 in TylHI. Because TylHI possesses an alanine at position 120 (equivalent to position 89 in MycCI), Arg-108 is pointed downward to interact primarily with Asp-248 and thus effectively adopts the functional role of Arg-89 in MycCI.

Given that Arg-77 was also determined to play some role in mediating binding of macrolactones to MycCI (see above), we generated and tested the $TylHI_{A120R}$ mutant with the hypothesis that the presence of a positively charged residue at position 120 of TylHI would promote $TylHI_{R108}$ to adopt an orientation more similar to that of $MycCI_{R77}$. Because only minor improvements in turnover were observed for the single mutant (Table S1), we opted to test the A120R mutation in the context of the $TylHI_{88-112}$ chimera, hoping that further extending the region replaced to residue 120 would lead to improved binding and conversion of all substrates, especially aglycones **11** and **12**. Although overall turnover dropped for $TylHI_{88-120}$ relative to $TylHI_{88-112}$ (Fig. 2*D*), binding of all substrates actually improved, even for compounds **10**, **11**, and **12** (Table 4). A time-course analysis performed with substrates **2** and **7** indicated that $TylHI_{88-112}$ most likely achieved higher turnovers than $TylHI_{88-120}$ due to a combination of overall faster catalytic rate and prolonged activity of the enzyme in the reaction mixture (Fig. S5).

Alignment of the amino acid sequences of MycCI, TylHI, and ChmHI showed three additional residues outside of the BC loop that are proximal (≤5 Å) to bound substrate and that are identical between MycCI and ChmHI but different from TylHI: $MycCI_{S161}$/$TylHI_{T192}$ located in the C-terminal portion of the F helix (SRS2), $MycCI_{S172}$/$TylHI_{A204}$ located in the N-terminal portion of the G helix (SRS3), and $MycCI_{I378}$/$TylHI_{V410}$ located in the C-terminal loop region after the L helix (SRS6) (Figs. 7 and S1*D*). Although the V410I substitution alone had no effect on substrate turnover or binding (Tables S1 and S2), a triple mutant designated $TylHI_{TAV}$ (denoting $TylHI_{T192S/A204S/V410I}$) exhibited improved activity across each of the tylosin-type macrolides tested (Fig. 2*D*). Especially notable was its improved capacity to hydroxylate **2** (65% conversion for $TylHI_{TAV}$ *versus* 40% conversion for WT) as well as the desosaminylated substrates **6**, **7**, and **9** (3–5-fold higher conversions relative to WT). Although binding of these substrates also markedly improved, **10** actually bound more poorly, whereas affinity with respect to **11** was left essentially unaltered (Table 4).

Given the enhancement in activity provided by these three additional mutations, we introduced them to each of the BC loop chimeras ($TylHI_{88-112}$, $TylHI_{103-107}$, and $TylHI_{88-120}$) to examine their effect in these different contexts. Indeed, turnover of all substrates with the exception of **10** improved in each case (Table S1). $TylHI_{88-112/TAV}$ was the most active among the three chimeras, exhibiting ≥81% conversion of mycaminosylated substrates **2**, **3**, and **8**; ≥67% conversion of desosaminylated substrates **6**, **7**, and **9**; 23% conversion of **10**; and 11% conversion of **11** (Fig. 2*D*). Although, like its WT parent, $TylHI_{TAV}$ was incapable of hydroxylating **11**, addition of these three mutations to the BC loop chimeras led to notable improvements in their ability to convert this aglycone. As expected, improved substrate turnover occurred in parallel with increased substrate binding affinity in all cases examined (Tables 4 and S2). However, despite its affinity toward **10** nearly doubling, $TylHI_{88-112/TAV}$ did not hydroxylate this compound to any greater extent relative to the parent

Table 4
Dissociation constants of selected substrates against TylHI/MycCI chimeras
K_d values are shown in μM. Reported errors are those obtained from fitting data averaged from experiments performed in duplicate.

TylHI/MycCI chimera	3	2	7	6	10	11	12
TylHI (wildtype)	0.63 ± 0.02	45 ± 3	236 ± 23	210 ± 8	925 ± 75	282 ± 16	401 ± 157
$TylHI_{88–112}$	41 ± 6	20 ± 2	41 ± 5	25 ± 2	16 ± 1	238 ± 24	479 ± 78
$TylHI_{103–107}$	2.1 ± 0.2	4.1 ± 0.3	29 ± 4	7.6 ± 0.7	157 ± 10	205 ± 32	ND[a]
$TylHI_{S107F}$	0.11 ± 0.04	3.3 ± 0.3	39 ± 6	14 ± 2	271 ± 30	178 ± 20	ND
$TylHI_{88–120}$	23 ± 1	9.5 ± 1.0	19 ± 2	8.8 ± 1.0	5.8 ± 0.7	195 ± 10	240 ± 34
$TylHI_{TAV}$	0.25 ± 0.08	9 ± 1	97 ± 5	109 ± 6	1444 ± 143	262 ± 10	ND
$TylHI_{88–112/TAV}$	15 ± 1	5.7 ± 0.6	16 ± 1	12 ± 1	9 ± 1	170 ± 11	210 ± 33
$TylHI_{88–112/192–206}$	1.7 ± 0.2	1.0 ± 0.1	1.7 ± 0.2	1.02 ± 0.10	2.5 ± 0.3	40 ± 2	210 ± 14

[a] ND, value not determined.

$TylHI_{88–112}$. Moreover, although the former was capable of binding **12** with an affinity similar to that of **11** (K_d for **12** = 210 μM), no products were observed. This result may relate to the fact that only ~20% of $TylHI_{88–112/TAV}$ was shifted to the high-spin state at saturating levels of **12** (Table S2).

In an attempt to produce an even more active P450 chimera that could catalyze hydroxylation of **12**, we elected to exchange the entire regions encompassing SRS1–3 (note that the residues making up SRS4 in the middle of the I helix and SRS5 in the loop right after the K helix are identical among MycCI, TylHI, and ChmHI; see Fig. 7). Creation of this chimera involved replacing residues 192–206 (referred to here as the "FG loop") in TylHI with the corresponding residues in MycCI and adding them to $TylHI_{88–112}$ to generate $TylHI_{88–112/192–206}$. Compared with the former, the latter BC/FG loop chimera was more active on every substrate tested. Most significantly, its conversion of **10** more than doubled to 45%, whereas it was capable of converting nearly an order of magnitude more **11** (24%) to the corresponding hydroxylated product. Strikingly, the dissociation constants for all tylosin-type macrolides were 1–2 μM, and that for mycinamicin-type macrolide **10** was 2.5 μM, representing a 370-fold increase in binding affinity relative to WT TylHI (Table 4). Affinity toward aglycone **11** was also considerably enhanced, with a K_d of 40 μM representing a 7-fold improvement over the WT enzyme and even surpassing the binding affinity of mycaminosylated substrate **2** toward the latter (Table 4). Although **12** bound with a K_d of 210 μM and shifted ~35% of the heme iron to the high-spin state upon saturation (Table S2), the BC/FG loop chimera was still unable to hydroxylate this aglycone. Moreover, even though $TylHI_{88–112/192–206}$ bound all of the substrates more tightly than did $TylHI_{88–112/TAV}$, the latter exhibited higher turnover activity across most of the compounds (with **10** and **11** serving as key exceptions), indicating that binding affinity does not always correlate with overall conversion.

Discussion

In the present study, we sought to gain an understanding of the specific factors governing the divergence in catalytic activity of two homologous cytochromes P450 involved in the biosynthesis of related 16-membered ring macrolide antibiotics. A combination of biochemical, structural, and computational approaches ultimately prompted the construction of several TylHI/MycCI chimeric P450s that proved critical for clarifying the roles of specific structural elements in tailoring the substrate specificity of these enzymes.

In P450s, the region between the B and C helices (*i.e.* the BC loop; may also include a short B′ helix) comprises an important substrate recognition site (SRS1) (43) and can strongly influence the substrate specificity of these enzymes (44). The BC loop exhibits a high level of variability in terms of both primary sequence and three-dimensional conformation among different P450 isoforms, features that are thought to influence the selectivity of these enzymes for a broad range of substrates (4, 44, 45). Significant movements involving the BC loop as well as the F/G helices and FG loop are associated with the open/close transitions of P450s that are implicated in substrate binding and catalysis (4, 44–47). Flexible loop regions such as these are responsible for sealing the active site to create a competent reaction chamber for substrate oxidation. The specific sequence and length of the BC loop in particular could significantly impact the ability of certain substrates to bind productively in the active site by influencing the conformational flexibility of this region of the enzyme prior to substrate binding as well as by dictating the identities of specific residues that come into contact with the substrate once it has bound (44, 46). It has been hypothesized that the presence of a sufficiently flexible BC loop is important for the ability of some bacterial P450s to bind large, bulky molecules such as macrolides (48, 49). Furthermore, computational and experimental evidence highlights the central role that the F/G helices and FG loop play in defining the properties of key substrate access channels in many P450s (45, 50). In turn, the nature of these access channels can have a major impact on P450 substrate specificity by mediating both substrate binding and product release (45, 50, 51).

The results of the present study support the roles of both the BC and FG loop regions in facilitating substrate binding for macrolide biosynthetic P450s. Although the MycCI BC loop was found to play a significant role in relaxing TylHI selectivity preferences for 16-membered ring substrates bearing different deoxyamino sugars, the synergistic combination of the BC and FG loop exchanges led to improved binding of substrates lacking a sugar moiety. Although the binding affinities of the desosaminylated substrates improved by more than two orders of magnitude for the TylHI BC/FG loop chimera relative to the WT enzyme, the dissociation constants never dropped below ~1 μM. Indeed, one question that remains unanswered relates to how MycCI is able to bind glycosylated substrates so tightly (*i.e.* in the low nanomolar range) (35). As essentially all of the residues that are located in proximity to bound substrate are identical between MycCI and the TylHI BC/FG loop chimera, regions of the protein outside of the active site must necessarily

be involved in the differences in catalytic behavior that remain between these two enzymes. In this context, it is worth considering that specific contacts established upon substrate binding may be of secondary importance to the rate at which substrate is able to bind, which is almost certainly dependent on the dynamics of not only the BC loop and F/G helices, but also other structural elements (45, 46).

Although our results may be applicable to many other P450 isoforms, the importance of the BC and FG loop regions for substrate binding and turnover may not always be apparent from an experimental perspective. Recently, Cryle and coworkers (52) investigated the divergent substrate specificity of the OxyB P450s from the vancomycin and teicoplanin biosynthetic pathways using an approach very similar to the one we employed in the present study. Although OxyB from the vancomycin pathway ($OxyB_{van}$) exhibits a rather broad substrate scope and is capable of accepting a variety of peptides tethered to peptidyl carrier proteins, the homolog from the teicoplanin pathway ($OxyB_{tei}$; 74% sequence identity) is much more discriminating and is unable to accept nonnative peptide substrates. Moreover, $OxyB_{tei}$ activity is highly dependent on an auxiliary nonribosomal peptide synthetase domain, which serves as a recruitment platform for the P450s that catalyze aryl and phenolic coupling reactions in the biosynthesis of glycopeptide antibiotics (53, 54). In the study, the BC loop and/or the F and G helices (including the FG loop) were transplanted from $OxyB_{van}$ to $OxyB_{tei}$, and the activities of the resulting chimeras were assessed (52). No gain-of-function activity was observed for these hybrids, indicating that the relaxed substrate specificity of $OxyB_{van}$ could not be attributed to these particular regions of the enzyme.

Finally, it is worth considering the evolutionary relationship between homologous yet functionally distinct enzymes like MycCI and TylHI. In nature as well as in laboratory evolution, a "generalist" enzyme capable of accepting a broad range of substrates with suboptimal efficiency often serves as an early intermediate en route toward a "specialist" that exhibits high activity on one or a few substrates (55, 56). Thus, one might hypothesize that MycCI represents a generalist intermediate in an evolutionary trajectory leading from one specialist enzyme to another, whereas TylHI is a specialist that has already reached its evolutionary "end point." However, the question of why MycCI displays a high level of activity on a range of substrates comparable to that of TylHI on its native substrate remains to be answered. Another intriguing question relates to the evolutionary history of the CYP105L subfamily of P450s, which includes MycCI, TylHI, ChmHI, and a few others. Is the common ancestor of these enzymes a generalist like MycCI or a specialist like TylHI? One may be tempted to answer in favor of the former, but the other option is certainly plausible. As the chimeragenesis experiments have demonstrated, it is quite feasible to produce a generalist from a specialist through the manipulation of a few key residues.

Conclusions

Through a synergistic combination of biochemical, structural, and computational experiments, we explored the molecular-level details underpinning the unique catalytic divergence of two homologous biosynthetic P450s involved in late-stage hydroxylation of macrolide antibiotics. Activity and binding assays employing substrate analogs revealed that mycaminose acts as a more important recognition element for TylHI than the aldehyde substituent of its native substrate. The crystal structure of this enzyme bound to the latter exhibited few differences from that of MycCI bound to its native substrate with the exception of the identities and relative positions/conformations of a few residues in the BC and FG loop regions. Several acidic and basic residues interacting to form a salt bridge network proximal to the deoxyamino sugar were shown by site-directed mutagenesis to play key roles in substrate binding and catalysis. However, few direct contacts with bound substrate were observed. Finally, the results of MD simulations and comparative analysis of a homologous P450 (ChmHI) aided in selecting specific regions of TylHI to replace with those of MycCI, enabling the generation of functional chimeras that provided new insight into the importance of the BC and FG loops in regulating the substrate flexibility of these two enzymes. This information may prove valuable in the rational design of new P450s with even broader substrate scope for use in the oxidative functionalization of macrolactones and other important molecular scaffolds.

Experimental procedures

Escherichia coli DH5α was used for plasmid preparation, maintenance, and propagation. Site-directed mutants and P450 chimeras were generated via whole-plasmid PCR amplification using mutagenic primers (Table S4a) and the vector containing WT TylHI as parent template. Proteins were expressed in *E. coli* BL21(DE3) and purified as described previously (35) with a few minor alterations. The TylHI/23-DMTL complex was crystallized by hanging-drop vapor diffusion. X-ray diffraction data were collected at beamline 8.3.1, Advanced Light Source, Lawrence Berkeley National Laboratory. The crystal structure was determined by molecular replacement using MycCI (PDB code 5FOI) as a search model. MT (**2**) was prepared in three steps starting from 23-DMTL (**3**). The latter was isolated from *S. fradiae* GS76 cultures as described previously (35). Compound **3** was first reduced to 20-OH-MT (**8**), and the hydroxyl group at C20 was removed via iodination and subsequent reduction to afford compound **2** (Scheme S1). All other substrates were prepared as described previously (35, 36). Analytical-scale enzymatic reactions and spectroscopic substrate binding assays were performed as described previously (35) with a few minor alterations. See the supporting information for additional experimental details.

Author contributions—M. D. D. and D. H. S. conceptualization; M. D. D., K. N. H., L. M. P., and D. H. S. supervision; M. D. D., N. L. S., S. Y., M. G.-B., and J. N. S. investigation; M. D. D. and S. Y. visualization; M. D. D. and S. Y. writing-original draft; M. D. D., K. N. H., L. M. P., and D. H. S. project administration; S. Y., M. G.-B., and J. N. S. software; K. N. H., L. M. P., and D. H. S. funding acquisition; D. H. S. writing-review and editing.

Acknowledgments—We thank Andrew Lowell (Virginia Tech) for assistance with substrate preparation and Wendy Feng (University of Michigan) for assistance with LC-MS data acquisition.

References

1. Brodie, B. B., Axelrod, J., Cooper, J. R., Gaudette, L., La Du, B. N., Mitoma, C., and Udenfriend, S. (1955) Detoxication of drugs and other foreign compounds by liver microsomes. *Science* **121,** 603–604 CrossRef Medline
2. Klingenberg, M. (1958) Pigments of rat liver microsomes. *Arch. Biochem. Biophys.* **75,** 376–386 CrossRef Medline
3. Garfinkel, D. (1958) Studies on pig liver microsomes. I. Enzymic and pigment composition of different microsomal fractions. *Arch. Biochem. Biophys.* **77,** 493–509 CrossRef Medline
4. Ortiz de Montellano, P. R. (ed) (2015) *Cytochrome P450: Structure, Mechanism, and Biochemistry*, 4th Ed., Springer, New York
5. Munro, A. W., Girvan, H. M., Mason, A. E., Dunford, A. J., and McLean, K. J. (2013) What makes a P450 tick? *Trends Biochem. Sci.* **38,** 140–150 CrossRef Medline
6. Meunier, B., de Visser, S. P., and Shaik, S. (2004) Mechanism of oxidation reactions catalyzed by cytochrome P450 enzymes. *Chem. Rev.* **104,** 3947–3980 CrossRef Medline
7. Denisov, I. G., Makris, T. M., Sligar, S. G., and Schlichting, I. (2005) Structure and chemistry of cytochrome P450. *Chem. Rev.* **105,** 2253–2277 CrossRef Medline
8. Guengerich, F. P. (2001) Common and uncommon cytochrome P450 reactions related to metabolism and chemical toxicity. *Chem. Res. Toxicol.* **14,** 611–650 CrossRef Medline
9. Cryle, M. J., Stok, J. E., and De Voss, J. J. (2003) Reactions catalyzed by bacterial cytochromes P450. *Aust. J. Chem.* **56,** 749–762 CrossRef
10. Isin, E. M., and Guengerich, F. P. (2007) Complex reactions catalyzed by cytochrome P450 enzymes. *Biochim. Biophys. Acta* **1770,** 314–329 CrossRef Medline
11. Guengerich, F. P., and Munro, A. W. (2013) Unusual cytochrome P450 enzymes and reactions. *J. Biol. Chem.* **288,** 17065–17073 CrossRef Medline
12. Kelly, S. L., Lamb, D. C., Jackson, C. J., Warrilow, A. G., and Kelly, D. E. (2003) The biodiversity of microbial cytochromes P450. *Adv. Microb. Physiol.* **47,** 131–186 CrossRef Medline
13. Lamb, D. C., Ikeda, H., Nelson, D. R., Ishikawa, J., Skaug, T., Jackson, C., Omura, S., Waterman, M. R., and Kelly, S. L. (2003) Cytochrome P450 complement (CYPome) of the avermectin-producer *Streptomyces avermitilis* and comparison to that of *Streptomyces coelicolor* A3(2). *Biochem. Biophys. Res. Commun.* **307,** 610–619 CrossRef Medline
14. Parajuli, N., Basnet, D. B., Chan Lee, H., Sohng, J. K., and Liou, K. (2004) Genome analyses of *Streptomyces peucetius* ATCC 27952 for the identification and comparison of cytochrome P450 complement with other *Streptomyces*. *Arch. Biochem. Biophys.* **425,** 233–241 CrossRef Medline
15. Podust, L. M., and Sherman, D. H. (2012) Diversity of P450 enzymes in the biosynthesis of natural products. *Nat. Prod. Rep.* **29,** 1251–1266 CrossRef Medline
16. Rudolf, J. D., Chang, C.-Y., Ma, M., and Shen, B. (2017) Cytochromes P450 for natural product biosynthesis in *Streptomyces*: sequence, structure, and function. *Nat. Prod. Rep.* **34,** 1141–1172 CrossRef Medline
17. Greule, A., Stok, J. E., De Voss, J. J., and Cryle, M. J. (2018) Unrivalled diversity: the many roles and reactions of bacterial cytochromes P450 in secondary metabolism. *Nat. Prod. Rep.* **35,** 757–791 CrossRef Medline
18. Fujii, Y., Hirosue, S., Fujii, T., Matsumoto, N., Agematu, H., and Arisawa, A. (2006) Hydroxylation of oleanolic acid to queretaroic acid by cytochrome P450 from *Nonomuraea recticatena*. *Biosci. Biotechnol. Biochem.* **70,** 2299–2302 CrossRef Medline
19. Kabumoto, H., Miyazaki, K., and Arisawa, A. (2009) Directed evolution of the actinomycete cytochrome P450 MoxA (CYP105) for enhanced activity. *Biosci. Biotechnol. Biochem.* **73,** 1922–1927 CrossRef Medline
20. Xue, Y., Wilson, D., Zhao, L., Liu H.-w., Sherman, D. H. (1998) Hydroxylation of macrolactones YC-17 and narbomycin is mediated by the *pikC*-encoded cytochrome P450 in *Streptomyces venezuelae*. *Chem. Biol.* **5,** 661–667 CrossRef Medline
21. Moody, S. C., and Loveridge, E. J. (2014) CYP105—diverse structures, functions and roles in an intriguing family of enzymes in *Streptomyces*. *J. Appl. Microbiol.* **117,** 1549–1563 CrossRef Medline
22. McGuire, J. M., Boniece, W. S., Higgens, C. E., Hoehn, M. M., Stark, W. M., Westhead, J., and Wolfe, R. N. (1961) Tylosin, a new antibiotic. I. Microbiological studies. *Antibiot. Chemother.* **11,** 320–327
23. Pape, H., and Brillinger, G. U. (1973) Metabolic products of microorganisms. 113. Biosynthesis of thymidine diphospho mycarose in a cell-free system from *Streptomyces rimosus*. *Arch. Mikrobiol.* **88,** 25–35 CrossRef Medline
24. Jensen, A. L., Darken, M. A., Schultz, J. S., and Shay, A. J. (1963) Relomycin: flask and tank fermentation studies. *Antimicrob. Agents Chemother.* **161,** 49–53 Medline
25. Seno, E. T., Pieper, R. L., and Huber, F. M. (1977) Terminal stages in the biosynthesis of tylosin. *Antimicrob. Agents Chemother.* **11,** 455–461 CrossRef Medline
26. Baltz, R. H., and Seno, E. T. (1981) Properties of *Streptomyces fradiae* mutants blocked in biosynthesis of the macrolide antibiotic tylosin. *Antimicrob. Agents Chemother.* **20,** 214–225 CrossRef Medline
27. Seno, E. T., and Baltz, R. H. (1981) Properties of *S*-adenosyl-L-methionine: macrocin *O*-methyltransferase in extracts of *Streptomyces fradiae* strains which produce normal or elevated levels of tylosin and in mutants blocked in specific *O*-methylations. *Antimicrob. Agents Chemother.* **20,** 370–377 CrossRef Medline
28. Seno, E. T., and Baltz, R. H. (1982) *S*-Adenosyl-L-methionine:macrocin *O*-methyltransferase activities in a series of *Streptomyces fradiae* mutants that produce different levels of the macrolide antibiotic tylosin. *Antimicrob. Agents Chemother.* **21,** 758–763 CrossRef Medline
29. Omura, S., Sadakane, N., and Matsubara, H. (1982) Bioconversion and biosynthesis of 16-membered macrolide antibiotics. XXII. Biosynthesis of tylosin after protylonolide formation. *Chem. Pharm. Bull.* **30,** 223–229 CrossRef
30. Omura, S., Tanaka, H., and Tsukui, M. (1982) Biosynthesis of tylosin: oxidations of 5-*O*-mycaminosylprotylonolide at C-20 and C-23 with a cell-free extract from *Streptomyces fradiae*. *Biochem. Biophys. Res. Commun.* **107,** 554–560 CrossRef Medline
31. Baltz, R. H., Seno, E. T., Stonesifer, J., and Wild, G. M. (1983) Biosynthesis of the macrolide antibiotic tylosin: a preferred pathway from tylactone to tylosin. *J. Antibiot.* **36,** 131–141 CrossRef Medline
32. Omura, S., Tomoda, H., Yamamoto, S., Tsukui, M., and Tanaka, H. (1984) Studies on two dioxygenases involved in the synthesis of tylosin in *Streptomyces fradiae*. *Biochim. Biophys. Acta* **802,** 141–147 CrossRef
33. Baltz, R. H., and Seno, E. T. (1988) Genetics of *Streptomyces fradiae* and tylosin biosynthesis. *Annu. Rev. Microbiol.* **42,** 547–574 CrossRef Medline
34. Cundliffe, E., Bate, N., Butler, A., Fish, S., Gandecha, A., and Merson-Davies, L. (2001) The tylosin-biosynthetic genes of *Streptomyces fradiae*. *Antonie Van Leeuwenhoek* **79,** 229–234 CrossRef Medline
35. DeMars, M. D., 2nd, Sheng, F., Park, S. R., Lowell, A. N., Podust, L. M., and Sherman, D. H. (2016) Biochemical and structural characterization of MycCI, a versatile P450 biocatalyst from the mycinamicin biosynthetic pathway. *ACS Chem. Biol.* **11,** 2642–2654 CrossRef Medline
36. Lowell, A. N., DeMars, M. D., 2nd, Slocum, S. T., Yu, F., Anand, K., Chemler, J. A., Korakavi, N., Priessnitz, J. K., Park, S. R., Koch, A. A., Schultz, P. J., and Sherman, D. H. (2017) Chemoenzymatic total synthesis and structural diversification of tylactone-based macrolide antibiotics through late-stage polyketide assembly, tailoring, and C–H functionalization. *J. Am. Chem. Soc.* **139,** 7913–7920 CrossRef Medline
37. Bate, N., Butler, A. R., Gandecha, A. R., and Cundliffe, E. (1999) Multiple regulatory genes in the tylosin biosynthetic cluster of *Streptomyces fradiae*. *Chem. Biol.* **6,** 617–624 CrossRef Medline
38. Bignell, D. R., Bate, N., and Cundliffe, E. (2007) Regulation of tylosin production: role of a TylP-interactive ligand. *Mol. Microbiol.* **63,** 838–847 CrossRef Medline
39. Haslinger, K., Maximowitsch, E., Brieke, C., Koch, A., and Cryle, M. J. (2014) Cytochrome P450 $OxyB_{tei}$ catalyzes the first phenolic coupling step in teicoplanin biosynthesis. *ChemBioChem* **15,** 2719–2728 CrossRef Medline
40. Ma, J., Wang, Z., Huang, H., Luo, M., Zuo, D., Wang, B., Sun, A., Cheng, Y.-Q., Zhang, C., and Ju, J. (2011) Biosynthesis of himastatin: assembly line and characterization of three cytochrome P450 enzymes involved in the

post-tailoring oxidative steps. *Angew. Chem. Int. Ed. Engl.* **50,** 7797–7802 CrossRef Medline

41. Zhang, H., Chen, J., Wang, H., Xie, Y., Ju, J., Yan, Y., and Zhang, H. (2013) Structural analysis of HmtT and HmtN involved in the tailoring steps of himastatin biosynthesis. *FEBS Lett.* **587,** 1675–1680 CrossRef Medline
42. Ward, S. L., Hu, Z., Schirmer, A., Reid, R., Revill, W. P., Reeves, C. D., Petrakovsky, O. V., Dong, S. D., and Katz, L. (2004) Chalcomycin biosynthesis gene cluster from *Streptomyces bikiniensis*: novel features of an unusual ketolide produced through expression of the *chm* polyketide synthase in *Streptomyces fradiae*. *Antimicrob. Agents Chemother.* **48,** 4703–4712 CrossRef Medline
43. Gotoh, O. (1992) Substrate recognition sites in cytochrome P450 family 2 (CYP2) proteins inferred from comparative analyses of amino acid and coding nucleotide sequences. *J. Biol. Chem.* **267,** 83–90 Medline
44. Hasemann, C. A., Kurumbail, R. G., Boddupalli, S. S., Peterson, J. A., and Deisenhofer, J. (1995) Structure and function of cytochromes P450: a comparative analysis of three crystal structures. *Structure* **3,** 41–62 CrossRef Medline
45. Cojocaru, V., Winn, P. J., and Wade, R. C. (2007) The ins and outs of cytochrome P450s. *Biochim. Biophys. Acta* **1770,** 390–401 CrossRef Medline
46. Pochapsky, T. C., Kazanis, S., and Dang, M. (2010) Conformational plasticity and structure/function relationships in cytochromes P450. *Antioxid. Redox Signal.* **13,** 1273–1296 CrossRef Medline
47. Poulos, T. L. (2003) Cytochrome P450 flexibility. *Proc. Natl. Acad. Sci. U.S.A.* **100,** 13121–13122 CrossRef Medline
48. Xu, L.-H., Fushinobu, S., Ikeda, H., Wakagi, T., and Shoun, H. (2009) Crystal structures of cytochrome P450 105P1 from *Streptomyces avermitilis*: conformational flexibility and histidine ligation state. *J. Bacteriol.* **191,** 1211–1219 CrossRef Medline
49. Sherman, D. H., Li, S., Yermalitskaya, L. V., Kim, Y., Smith, J. A., Waterman, M. R., and Podust, L. M. (2006) The structural basis for substrate anchoring, active site selectivity, and product formation by P450 PikC from *Streptomyces venezuelae*. *J. Biol. Chem.* **281,** 26289–26297 CrossRef Medline
50. Urban, P., Lautier, T., Pompon, D., and Truan, G. (2018) Ligand access channels in cytochrome P450 enzymes: a review. *Int. J. Mol. Sci.* **19,** E1617 CrossRef Medline
51. Winn, P. J., Lüdemann, S. K., Gauges, R., Lounnas, V., and Wade, R. C. (2002) Comparison of the dynamics of substrate access channels in three cytochrome P450s reveals different opening mechanisms and a novel functional role for a buried arginine. *Proc. Natl. Acad. Sci. U.S.A.* **99,** 5361–5366 CrossRef Medline
52. Brieke, C., Tarnawski, M., Greule, A., and Cryle, M. J. (2018) Investigating cytochrome P450 specificity during glycopeptide antibiotic biosynthesis through a homologue hybridization approach. *J. Inorg. Biochem.* **185,** 43–51 CrossRef Medline
53. Haslinger, K., Peschke, M., Brieke, C., Maximowitsch, E., and Cryle, M. J. (2015) X-domain of peptide synthetases recruits oxygenases crucial for glycopeptide biosynthesis. *Nature* **521,** 105–109 CrossRef Medline
54. Peschke, M., Gonsior, M., Süssmuth, R. D., and Cryle, M. J. (2016) Understanding the crucial interactions between cytochrome P450s and nonribosomal peptide synthetases during glycopeptide antibiotic biosynthesis. *Curr. Opin. Struct. Biol.* **41,** 46–53 CrossRef Medline
55. Tracewell, C. A., and Arnold, F. H. (2009) Directed enzyme evolution: climbing fitness peaks one amino acid at a time. *Curr. Opin. Chem. Biol.* **13,** 3–9 CrossRef Medline
56. Khersonsky, O., Roodveldt, C., and Tawfik, D. S. (2006) Enzyme promiscuity: evolutionary and mechanistic aspects. *Curr. Opin. Chem. Biol.* **10,** 498–508 CrossRef Medline
57. Robert, X., and Gouet, P. (2014) Deciphering key features in protein structures with the new ENDscript server. *Nucleic Acids Res.* **42,** W320–W324 CrossRef Medline